SIT-P206 (1/68)

UNCLASSIFIED

DEPARTMENT OF PHYSICS

AN EXPERIMENTAL AND THEORETICAL INVESTIGATION OF TURBULENCE INSTABILITIES AT PLASMA-MAGNETIC FIELD INTERFACES

Semi-Annual Report

April 1967

and

Final Report

January 1968

Winston H. Bostick

NASA Grant #NsG-596

Office of Research Grants and Contracts

Code SC, National Aeronautics and Space Admin.

1520 H Street, N. W.

Washington, D. C. 20546

STEVENS INSTITUTE OF TECHNOLOGY

CASTLE POINT STATION

HOBOKEN, NEW JERSEY 07030

SIT-P206 (1/68)

UNCLASSIFIED

Stevens Institute of Technology
Department of Physics
Castle Point Station
Hoboken, New Jersey

An Experimental and Theoretical Investigation of Turbulence Instabilities at Plasma-Magnetic Field Interfaces

Semi-Annual Report
April 1967
and
Final Report
January 1968

Winston H. Bostick

NASA Grant #NsG-596

Office of Research Grants and Contracts
Code SC, National Aeronautics and Space Admin.
1520 H Street, N. W.
Washington, D. C. 20546

An Experimental and Theoretical Investigation of Turbulence Instabilities at Plasma-Magnetic Field Interfaces

Winston H. Bostick

Perpendicular-to-B_o Plasma Vortices in the Plasma Coaxial Accelerator

A new capacitor bank (10 kilojoules, 5 to 20 kV) and a new coaxial accelerator (4" and 2" in diameter) which is larger than the previous one are now in operation. Figures 1, 2, 3, and 4 taken in the light of H_β show the $\perp$-to-B_o plasma vortices being formed in pairs at the end of the center conductor of the coaxial accelerator. The peak current of 700 ka in the accelerator is occurring approximately at the time the discharge comes off the end of the center conductor. The pressure in the discharge tube is 8 mm and the gas is H_2. The appearance of these radial striations is essentially the same with either polarity on the coaxial accelerator. The spacing between the pairs can be seen to decrease as they are compressed toward the center of the end of the center conductor. The spacing between them varies inversely as the magnetic field. Measurements are also underway to measure the spacing as a function of the original gas density in the discharge tube. These $\perp$-to-B_o vortices are a kind of orthogonal flute in which the deformation which occurs in the plasma-magnetic field interface involves a bending of the field lines into flute-like pockets, where the axis of these flutes is perpendicular to the magnetic field. In the case of the plasma coaxial accelerator the current sheet becomes somewhat bullet-shaped and thus there is a flow of mass across the field lines along the axis of the orthogonal flutes. This flow across the field lines perhaps

discourages the formation of ordinary flute instability at the interface and encourages the formation of the orthogonal flutes.

Figure 5 is an attempt to diagram the formation of the orthogonal flutes (which become vortices) which occur when there is a pocket in the magnetic field. If as figure 6 shows, there is initially an unperturbed magnetic field with pressure $\frac{B^2}{8\pi}$ producing snow-plow action on a momentum density flow $n\, m_i\, \vec{v}\cdot\vec{v}$, Newton's second law gives $\frac{B^2}{8\pi} = n\, m_i v^2$ for the process of stopping the mass flow (in the frame of reference of the current sheath). However, the kinetic energy flow $\frac{1}{2}\, n\, m_i\, v^2 \cdot v$ must be accounted for. We will assume that this kinetic energy density flow in the steady state on an unperturbed plasma-magnetic field interface deposits a fraction of itself in the form of a steady-state pressure knT. Let us then write Newton's second law as

$$n\, m_i\, v^2\, (1 + \alpha) = \frac{B_o^2}{8\pi} \qquad (1)$$

The number α represents the effect of that pressure. In a perturbation in the magnetic field lines, such as is shown in figure 6, kinetic energy flow, which ends up as the pressure represented by α, now is deflected at the slopes in B in the regions corresponding to $kz = \pm\frac{\pi}{2}$ or $z = \pm\frac{\pi}{2_k} = \pm\frac{\lambda}{4}$. This energy is deposited in the pockets until the increased pressure in the pockets, $n\, m\, v^2\, \alpha\ \left(\frac{\lambda}{2}\ /_{l_{cm}}\right)$, is equal to the increase in magnetic field pressure at the pockets:

$$B \underset{y\,\simeq o}{\simeq} \frac{B_o}{2}\left(1 + \frac{y_o}{y_s}\cos kz\right) = \frac{B_o}{2}\,(1 + \Delta)$$

$$\frac{B^2}{8\pi} = \frac{B_o^2}{4 \cdot 8\pi} \left(1 + \frac{2y_o}{y_s} \cos kz + \ldots \right)$$

$$y \simeq o$$

$$\Delta \left(\frac{B_o^2}{8\pi} \right) = \frac{1}{8\pi} \frac{1}{2} \left(\frac{B_o}{2} \right) \Delta B = \frac{1}{8\pi} \frac{B_o}{4} \frac{y_o}{y_s} \cos kz \qquad (2)$$

$$y \simeq o$$

Then we write $n m_i v^2 \alpha \left(\frac{\lambda}{2} \right) = \frac{1}{8\pi} \frac{B_o^2}{4} \frac{y_o}{y_s} \cos kz \qquad (3)$

This equation shows that for large momentum flows the magnetic field B_o must be high and the gradient B_o/y_s must be high. Also, the larger the value of $\frac{\lambda}{2}$, the larger the expected amplitude y_o. This model must be refined so that we can obtain growth rates of the amplitude and a prediction of the equilibrium wave length as a function of the magnetic field and the momentum flow.

Transverse-to-magnetic-field filamentary structure (figs. 7, 8, 9 and 10) was also observed in a lithium plasma streaming into a magnetic field gradient produced by an axial current. The filament was found to be lying in a plane passing through the axial conductor and the button gun which was the plasma source. The typical densities in the filament were $10^{13}/cm^3$ and the velocities of the ions were $\sim 10^7$ cm/sec. The magnetic field at the bottom of the filament was 11,000 Gauss (at r = 0.5 cm).

The filament was observed to form very quickly and then it was observed to be repelled gradually away from the line current as a whole, stable filament structure. The body currents in the filament very likely are responsible for this high stability. A theoretical explanation of this phenomena is being worked out.

b. Parallel-to-B_o Plasma Vortices

The use of the plasma camera to measure the distribution of plasma in a magnetic field when a small two-wire button gun is fired across the field has now been developed into a tool which can yield valuable information. Figures 11, 12, 13 and 14 are examples of the photographs taken under the various conditions described in the captions. The patterns are so complex that they undoubtedly cannot be unraveled with probes alone, although probes have shown that the plasma circulated (rotates) as it translates across the field.

Conclusion:

The complexity of the plasma-magnetic field interface should not be underestimated. The work here at Stevens has shown that the appearance of perpendicular-to-B_o plasma vortices in the current sheath of the plasma coaxial accelerator (at pressures greater than 2 mm) is the most striking feature of the entire current sheath. That these vortex structures are minimum energy configurations there can be no doubt. However, to show analytically that these vortices are minimum energy states, to predict and measure their density, flow, and magnetic profiles is a research program for years to come.

The research work at Stevens with probes and the plasma camera on plasma moving across a homogeneous magnetic field shows that the parallel-to-B_o plasma vortex structure can be extremely complex at low magnetic fields. At magnetic fields above 1000 gauss the plasma assumes a much more regular shape and apparently rolls like a catapillar tractor track as it moves across the field. This behavior also must be understood analytically and this is a research program for years to come.

The firing of a two-wire button plasma gun into a magnetic field with a gradient produces not only a curved trajectory for the plasma, but the plasma ends up in a perpendicular-to-B_o vortex structure. To understand this complex process analytically is a program for years to come. The experiments thus far show in a semi-quantitative way how "minimum B" works as a containment device: The trajectories of the blobs of plasma in the gradient fields are curved by $\vec{j} \times \vec{B}$ forces. The current loops of the current density $\vec{j}$ can be drawn in a semi-quantitative way. To this extent the process can now be understood.

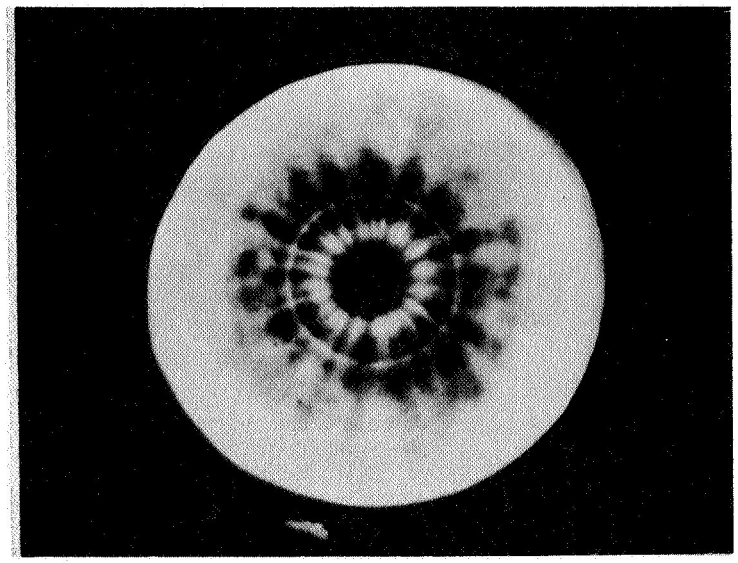

Figure 1

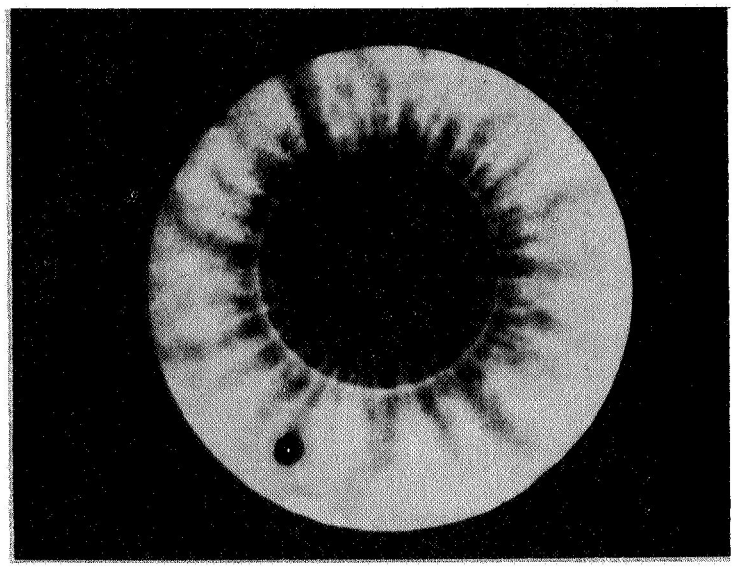

Figure 2

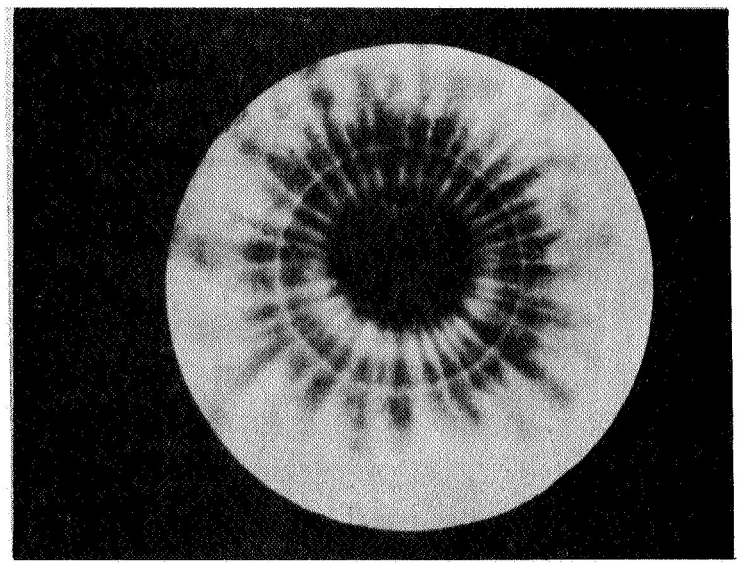

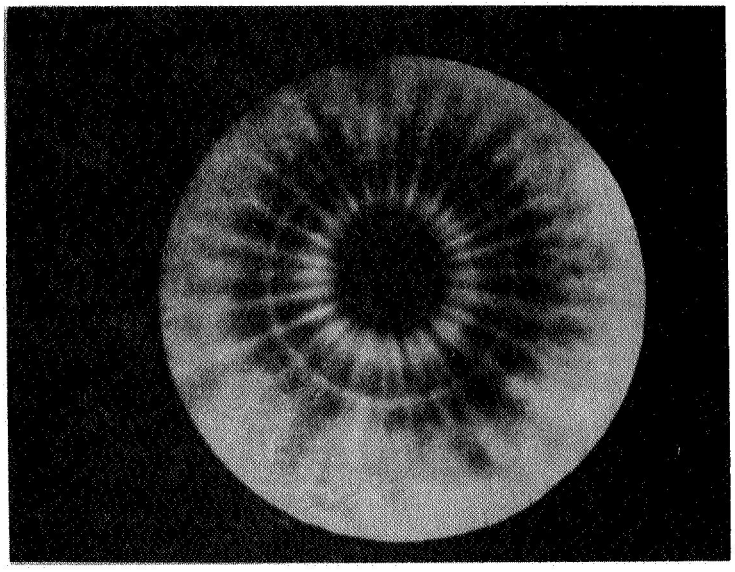

Figures 3a and 3b

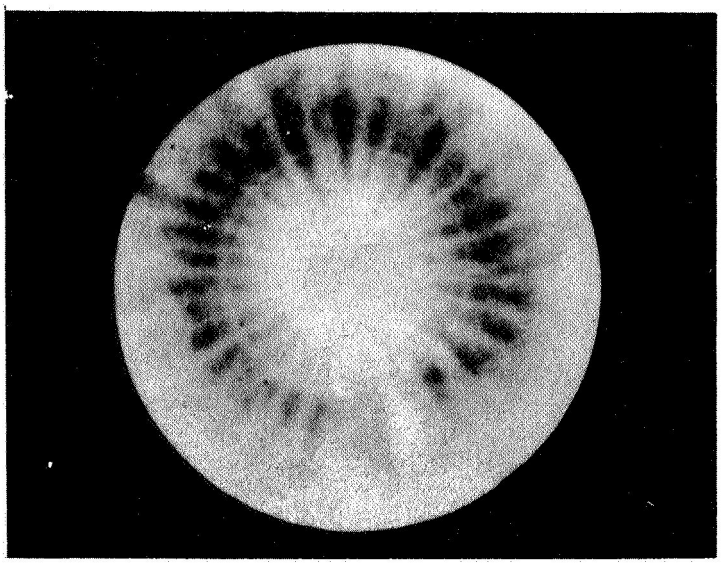

Figure 4

Figures 1, 2, 3a and b and 4 taken in the light of H_β showing the $\perp$-to-B_o plasma vortices being formed in pairs at the end of the center conductor of the coaxial accelerator. The five pictures show the vortices as they just roll off the center conductor to the final pinch. In the last picture the pinch region is over-exposed to show the filaments.

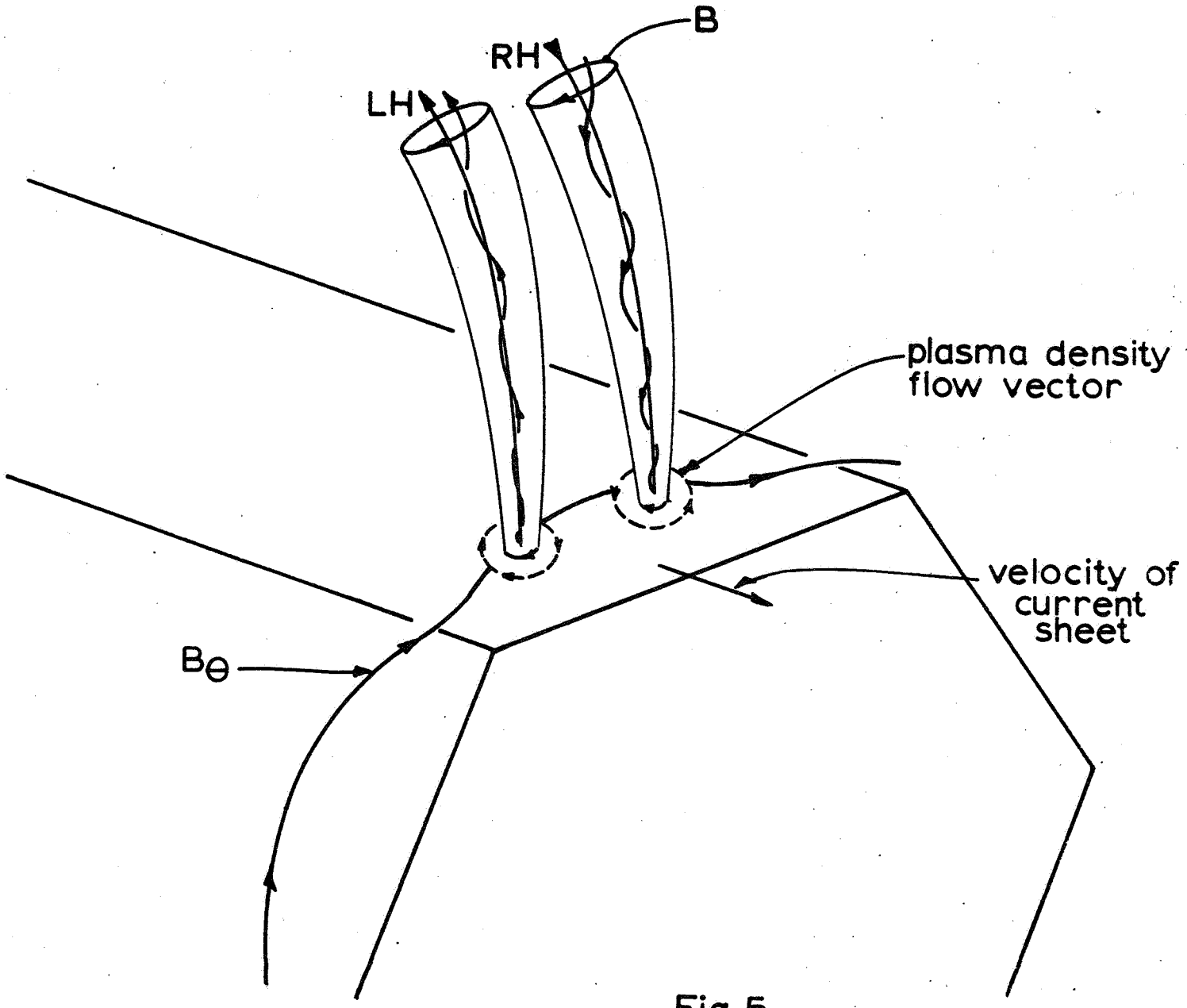
B
RH
LH
plasma density
flow vector
velocity of
current
sheet
B_θ

Fig.5

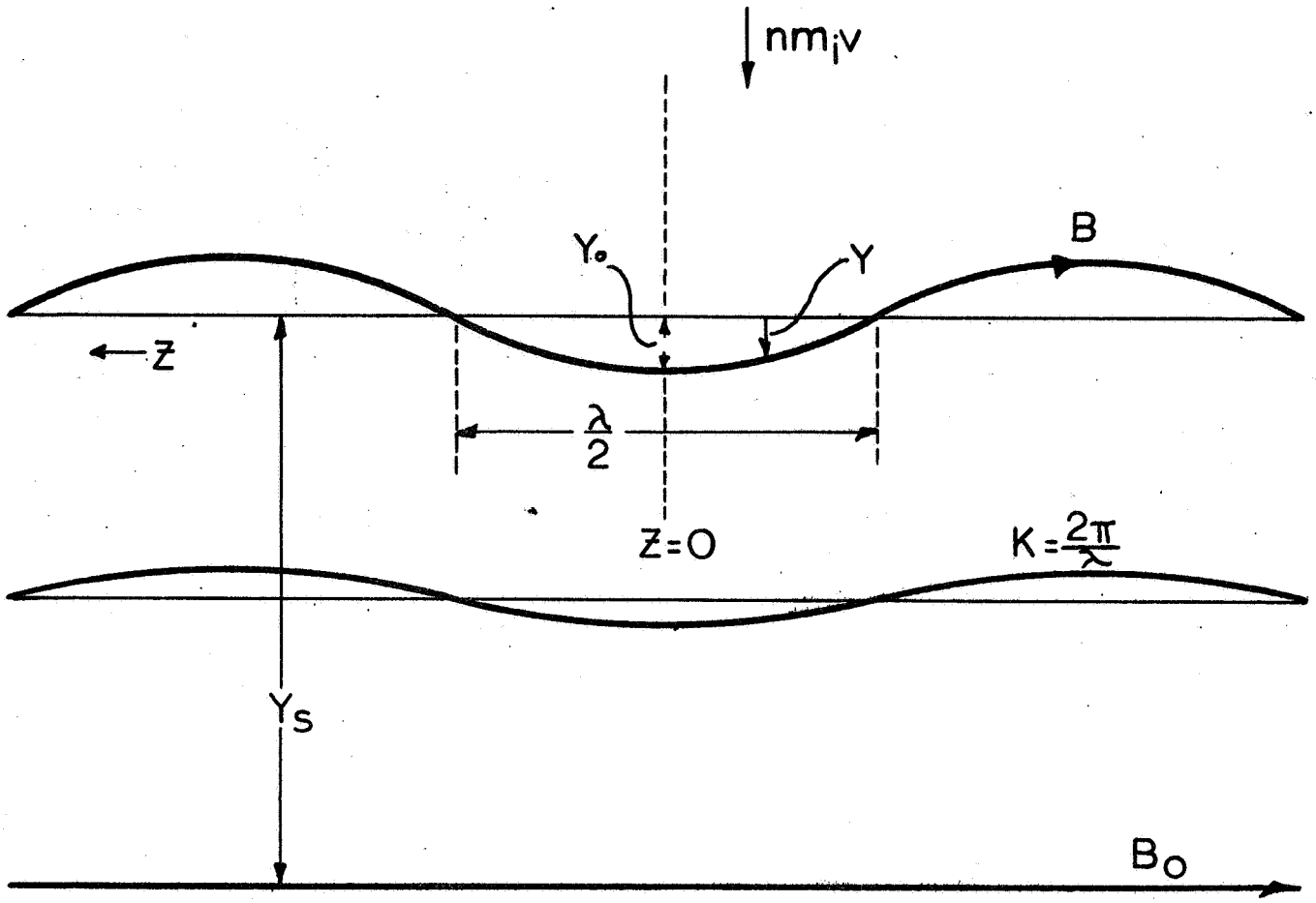

FIG. 6

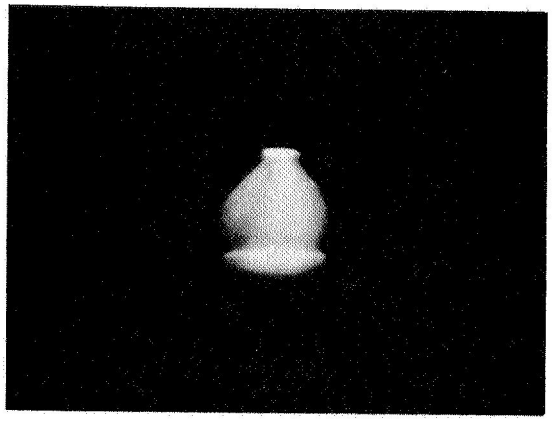

Figure 7

Typical Li-Button Gun firing in a zero external magnetic field. This is a time exposure photograph taken by the image converter camera. Illuminated axial conductor can be seen in the foreground. The gun period is a 0.7 μsec pulse of ∿ 1000 amp current. Background air pressure is 8×10^{-6} mm of mercury.

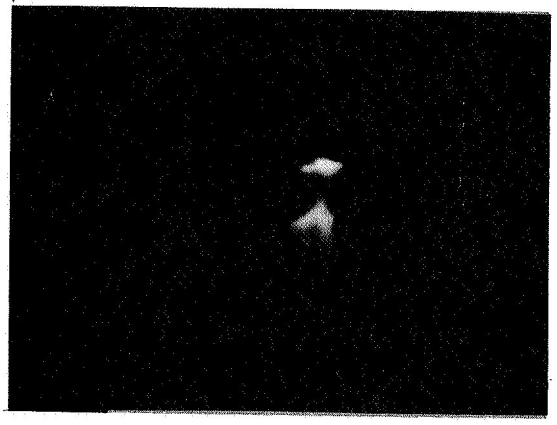

Figure 8

The Li-Gun fired into the magnetic field gradient. B $\left(\sim \frac{1}{r}\right)$ at the bottom of the filament is ∿ 11,000 Gauss and is out of the paper. The photograph is taken with the exposure time of 50 nsec at 0.6 μsec after the instant of the peak current in the gun. The ion velocities in plasma are ∿ 10^{7} cm/sec.

Figure 9

Same conditions as in fig. 8; except the picture is taken after a further delay of 0.2 μsec. Notice the gradual displacement of the filament away from the axial current.

Figure 10

Here the background pressure (air) is increased to 10^{-4} mm of mercury. The filament no longer has a simple forum. The decrease in the average ion velocities and the increase in the background neutral densities were found to be causing this complex behavior of the filament.

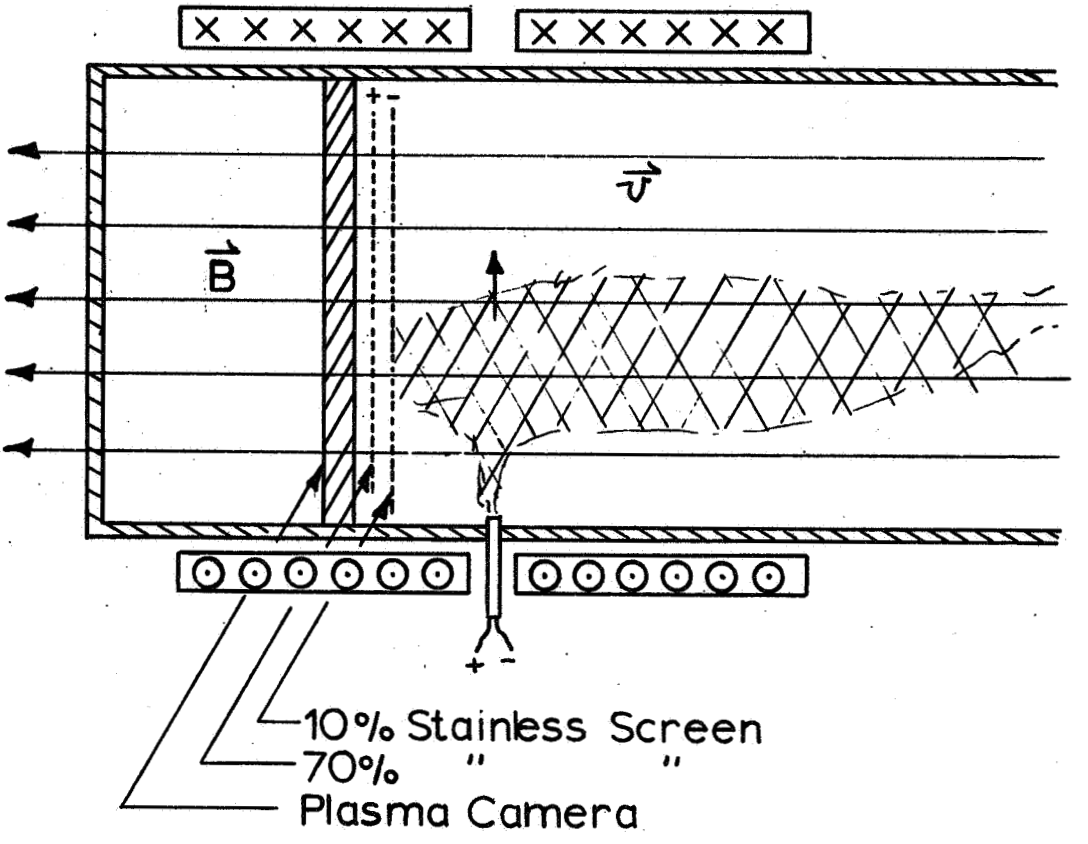

Figure 11

Drawn above is the experimental arrangement with the plasma camera. Plasma which moves across and along the magnetic field reaches the region of the camera. The stainless steel grids are pulsed, through an isolation transformer, with 10 kV. Electrons from the plasma are driven into an aluminized NE102 plastic scintillator which is photographed with an open shutter camera. The light pattern is thus representative of the plasma configuration near the surface of the camera at time of the pulse.

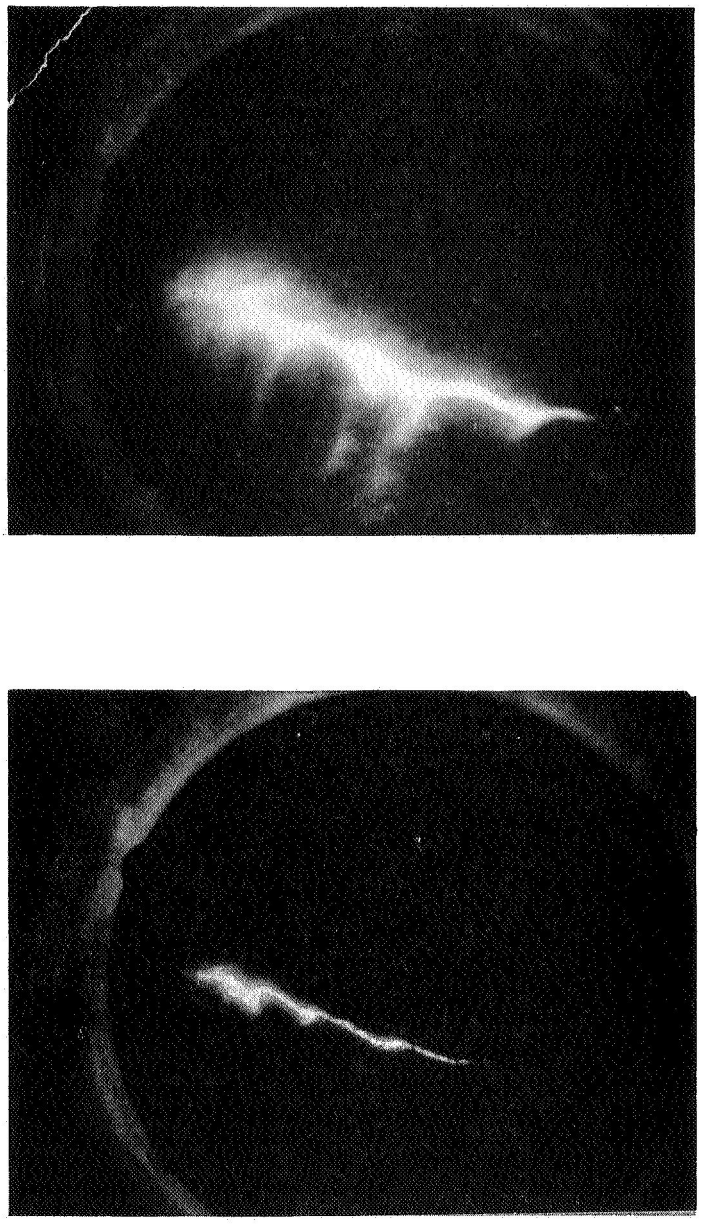

Figure 12

Plasma from Lead (Pb) electrodes is injected toward the right in magnetic fields of 400 Gauss (photo A) and 2400 Gauss (photo B). Density is about 10^{11} - 10^{12}/cc and $T_e \sim 5eV$. Exposures of .1 μsec were taken 2.4 μsec after firing of the gun. The field goes into the plane of the photographs and thus we see the "arms" of plasma which develop are in the $-\vec{v} \times \vec{B}$ direction. The "arms" are most noticable at low fields.

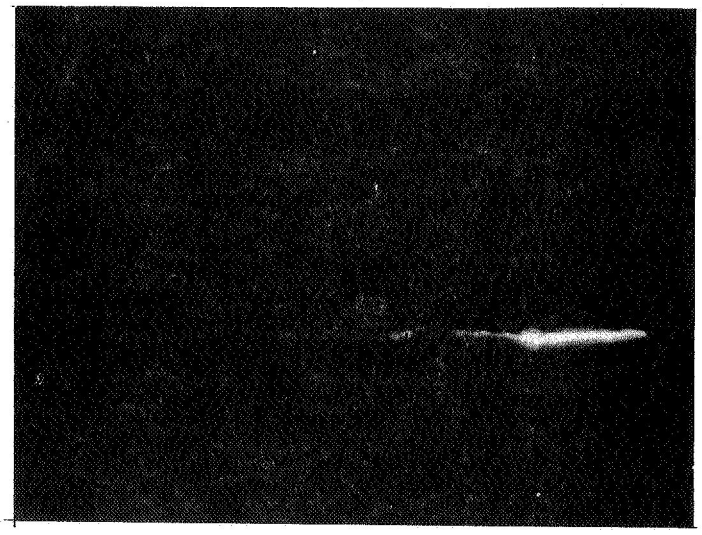

Figure 13

Here plasma from Lithium electrodes is substituted for the Lead plasma in the previous Figure 12. All conditions are the same and again plasma "arms" are seen to develop in the $-\vec{v} \times \vec{B}$ direction at low fields.

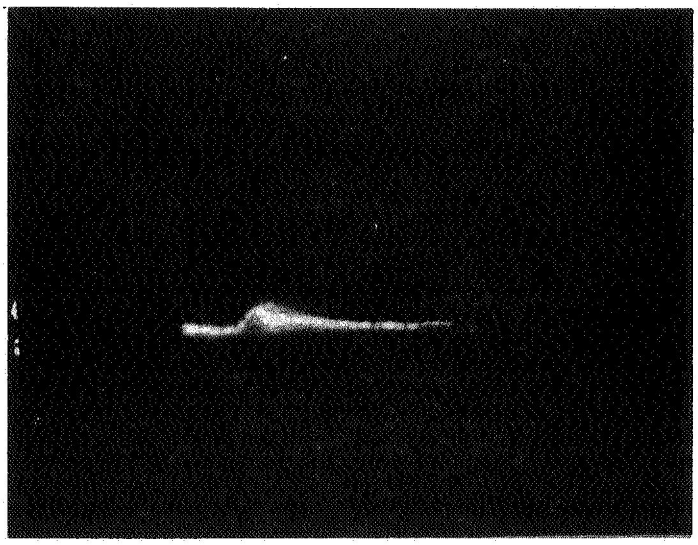

Figure 14

Plasma from Copper electrodes is injected from the right in magnetic fields of 400 and 2400 Gauss. (photos A and B respectively) The magnetic field here is out of the plane of the photograph and thus we see "arms" again develop in the $-\vec{v} \times \vec{B}$ direction. In photo B an unexplained though reproducible undulation is seen.